Simulation framework for reflective PPG signal analysis depending on sensor placement and wavelength

Maximilian Reiser
HAW Landshut & FAU Erlangen-Nürnberg
Landshut, Germany
maximilian.reiser@haw-landshut.de

Andreas Breidenassel
HAW Landshut
Landshut, Germany
andreas.breidenassel@haw-landshut.de

Oliver Amft
University of Freiburg, Germany
Hahn-Schickard, Germany
amft@ieee.org

***Abstract*—We analyse the influence of reflective photoplethysmography (PPG) sensor positioning relative to blood vessels. A voxel based Monte Carlo simulation framework was developed and validated to simulate photon-tissue interactions. An anatomical model comprising a multi-layer skin description with a blood vessel is presented to simulate PPG sensor positioning at the volar wrist. The simulation framework was validated against standard test cases reported in literature. The blood vessel was considered in regular and dilated states. Simulations were performed with 10^8 photon packets and repeated five times for each condition, including wavelength, relative position of PPG sensor and vessel, and vessel dilation state. Statistical weights were associated to photon packets to represent absorption and scattering effects. A symmetrical arrangement of the PPG sensor around the blood vessel showed the maximum AC signal. When the PPG sensor was not centrally placed over the vessel, simulated photon weight in systolic and diastolic state deteriorated by $\geq$5% for both wavelengths. With a position-dependent variation of $\geq$5% at 660 nm and $\geq$12% at 940 nm of light absorption, blood had the most profound effect on signal quality. The mean penetration depth is dependent on the blood vessel position for both wavelengths. Our simulation results demonstrate the susceptibility of reflective PPG measurement to interference and could explain wearable PPG sensor performance variations related to positioning and wavelength.**

***Index Terms*—photon-tissue interaction, dilated blood vessel, photon packets, signal quality, radial artery, wearable sensor**

I. Introduction

Recording the photoplethysmographic (PPG) curve is a non-invasive optical method to monitor vital parameters with wearable devices. A light source and a photodetector at the skin surface measure volumetric changes in blood circulation due to the heartbeat. Wrist-worn PPG devices are the most popular reflective PPG sensors for non-clinical monitoring [1]. In a reflective geometry, an adequate distance between source and detector is crucial. As wavelength increases, photon penetration depth [2] and optimal source-detector distance increases too. Moreover, PPG measurements are sensitive to shifts in sensor position and thus light path [1]. In this paper, we investigate PPG sensor positioning using Monte Carlo (MC) photon packets simulations and a realistic anatomical model. In particular, the following contributions are made:

1) We describe a full modelling stack from geometric and optical properties of the tissue to photon trajectories, light source and detector. We implemented and validated a voxel-based photon simulation framework to investigate PPG sensor positioning.
2) We analyse the PPG signal effects in relation to a large blood vessel, considering regular and dilated vessel structures to describe heartbeat. We provide results for wavelength, relative position and vessel state.

The work was partially funded by the Bavarian Academic Forum (BayWISS) Joint Academic Partnership "Health" and the Bavarian State Ministry of Science and the Arts.

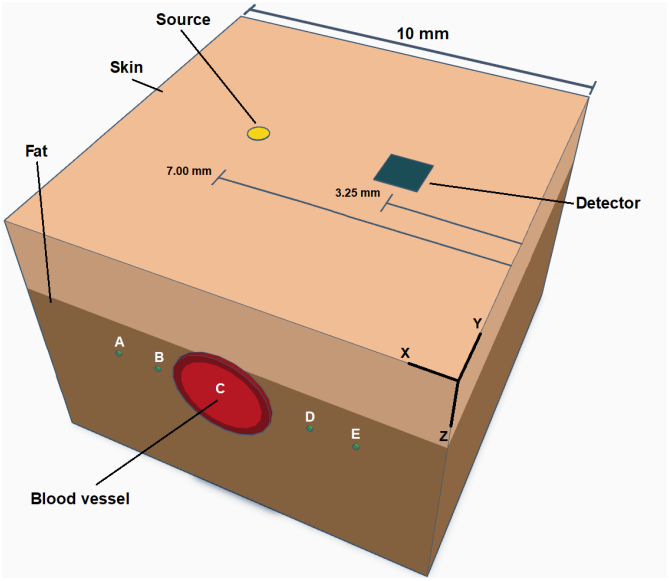

Fig. 1. Illustration of the simulated anatomical model. Individual skin layers were omitted from this illustration. Positions A-E mark alternative blood vessel positions considered in our simulation. Position C (shown) was the centred vessel position between light source and detector. Coordinate system origin was defined at the lower right corner of the anatomical model.

II. Methodology

To model and simulate photon-tissue interactions a MC simulation framework was developed based on previous work

of Wang et al. [3] and Fang et al. [4]. Our anatomical model was based on [5], consisting of skin and fat layers as well as a cylindrical blood vessel. For convenience of the simulation, a PPG measurement device was virtually positioned at a fixed skin surface. Blood vessel location was varied, resulting in five relative device-vessel positions.

A. Anatomical model

The anatomical model (see Fig. 1) represents the PPG measurement in a wearable at the volar wrist (inner or palm side of the wrist), centered over a radial artery. Skin was subdivided into six sublayers (*Stratum corneum*, *Epidermis*, *Papillary dermis*, *Upper blood net dermis*, *Reticular dermis* and *Deep blood net dermis*). Thickness t of all skin layers are listed in Tab. I. Every person's anatomy differs by gender, age, weight, or body composition, among other factors. For this reason, average values were used according to [5]. Our voxel representation of the anatomical model had a size of $10x10x7\,mm$ and a resolution of $0.01\,mm$ per voxel. Light source and detector were located at positions $[7.00, 5.00, 0]$ and $[3.25, 5.00, 0]$, respectively. The blood vessel represents an artery with a diameter of $d = 2.4\,mm$ [6], consisting of a vessel wall ($t = 0.2\,mm$ [7]) and blood (radius $r = 1.0\,mm$ [6]). Dilation of the blood vessel was realised by expanding the blood ($r = 1.2\,mm$) while maintaining a constant vessel wall. The artery was located at a depth of $3.00\,mm$ according to [8] and spanned across the y-axis. The blood vessel was simulated at position A ($x = 8.00\,mm$), B ($x = 7.00\,mm$), C ($x = 5.00\,mm$), D ($x = 3.25\,mm$), and E ($x = 2.25\,mm$).

B. Monte Carlo Simulation

The MC simulation was based on the principle of absorption and scattering of photons in tissue. Absorption coefficients μ_a indicate the probability of attenuation of photons bundled in a packet with a certain weight w. Scattering coefficients μ_s describe the probability of a scattering event during photon propagation in tissue. The MC simulation was divided into a sequence of steps, which are briefly described here. First, a photon packet was sent into tissue. As a source, a collimated Gaussian beam incidence was simulated according to a probability distribution, where b is the $1/e^2$ radius [3]:

$$p(r) = \frac{e^{\frac{-r^2}{b^2}} 2r}{b^2}. \tag{1}$$

Before entering the tissue, statistical weights w of all photon packet were set $w = 1$. First, specular reflection R_s was calculated using the Fresnel equation [3]:

$$R_s = \left(\frac{n_i - n_t}{n_i + n_t}\right)^2, \tag{2}$$

where n is the refractive index (i: incident, t: transmitted). The weight w of each photon packet entering the tissue was reduced by $R_s \cdot w$. Subsequently, the photon packet was sent through tissue with a step length l:

$$l = -\frac{\ln(\xi)}{\mu_s}, \tag{3}$$

where ξ is a uniformly distributed random number between 0 and 1. The photon packet was propagated through the tissue until it either hit a tissue border or it reached step length l. In the first case, the travelled length Δl was set to the distance to next border, otherwise it was set to step length l. At either event, weight w of the photon packet was updated by Lambert-Beer's law:

$$w = w \cdot e^{-\mu_a \, \Delta l}. \tag{4}$$

When hitting a border, Δl was updated by $\Delta l = l - \Delta l$. Otherwise a new step length l was calculated. At the end of the step length l a new scattering angle θ was calculated using the Henyey-Greenstein phase function [9]:

$$p(\theta) = \frac{1}{4\pi} \frac{1 - g^2}{(1 + g^2 - 2g\ cos\theta)^{\frac{3}{2}}}, \tag{5}$$

where g is the anisotropy factor. The azimuth angle ϕ was chosen randomly between 0 and 2π. If the photon packet transferred into another tissue, R [3] was calculated depending on the entrance angle θ_i and critical angle $\theta_c = sin^{-1}\frac{n_i}{n_t}$:

$$R = \begin{cases} \frac{(n_i - n_t)^2}{(n_i + n_t)^2} & \text{if } \theta_i = 0, \\ \frac{1}{2}\left[\frac{sin^2(\theta_i - \theta_t)}{sin^2(\theta_i + \theta_t)} + \frac{tan^2(\theta_i - \theta_t)}{tan^2(\theta_i + \theta_t)^2}\right] & \text{if } 0 < \theta_i < \theta_c, \\ 1 & \text{if } \theta_c < \theta_i < \frac{\pi}{2}. \end{cases} \tag{6}$$

If R is smaller as a randomly generated number ξ the photon packet was transmitted, otherwise it was reflected. The photon packets propagated through the anatomical model until they hit the skin surface or $w < 10^{-4}$. If the latter occurred, the Russian roulette technique [3] was used to simulate the energy conservation principle. The photon packet had a chance of 1:10 to tenfold its weight. After exiting the tissue, photon packets were assumed to be detected within the detector's surface area, otherwise discarded. Subsequently, the simulation continued with a new photon packet launched until the maximum number of photon packets to be simulated was reached.

C. Parameters

Absorption coefficients μ_a were derived as in [5]. Venous oxygen saturation was set 10% below arterial saturation. Epidermal melanin concentration was 10%. Scattering coefficients μ_s, tissue-dependent anisotropy factors g, and refractive indices n are taken from literature [7], [10]–[12], see Tab. I.

D. Validation

The developed MC model was validated based on data, published by [13] and [14]. Four test cases were investigated and compared with results of [13]–[15]. Ten MC simulations with 5000 photon packets were performed for each test case. Case 1 described a semi-infinite slab with optical parameters $n_i = 1.0$, $n_t = 1.5$, $\mu_a = 1.0\,mm^{-1}$, $\mu_s = 9.0\,mm^{-1}$ and isotropic scattering ($g = 0$). The reflection R at the top of the slab was recorded. Case 2 described a slab of turbid medium with a thickness of 0.02 mm. The optical parameters were $n_i = n_t = 1.0$, $\mu_a = 1.0\,mm^{-1}$, $\mu_s = 9.0\,mm^{-1}$ and $g = 0.75$. Both reflection R and transmission T were derived.

TABLE I
SKIN LAYERS OF OUR ANATOMICAL MODEL, INCLUDING MECHANICAL AND OPTICAL PARAMETER.

Layer	**Thickness** $[mm]$	$\mu_s\ [mm^{-1}]$		$\mu_a\ [mm^{-1}]$		**g [-]**	**n [-]**
		660 nm	***940 nm***	***660 nm***	***940 nm***		
Stratum corneum	0.02	22.33	9.50	0.082	0.072	0.86	1.51
Epidermis	0.08	22.33	9.50	2.731	0.847	0.80	1.34
Papillary dermis	0.16	22.33	9.50	0.034	0.046	0.90	1.41
Upper blood net dermis	0.08	22.33	9.50	0.082	0.208	0.95	1.38
Reticular dermis	1.50	22.33	9.50	0.024	0.048	0.80	1.35
Deep blood net dermis	0.08	22.33	9.50	0.036	0.085	0.95	1.38
Subcutaneous fat	5.00	11.40	10.99	0.026	0.055	0.75	1.44
Vessel wall	0.20	23.00	23.00	0.080	0.080	0.90	1.40
Blood[a]	2.00 (2.20)	87.61	66.08	0.150	0.650	0.98	1.40
Water	-	-	-	0.00041	0.0267	-	-

[a]Dilated diameter is shown in parentheses.

TABLE II
VALIDATION RESULTS OF THE MC SIMULATION FRAMEWORK WITH ANALYTICAL AND SIMULATED RESULTS.

Case 1				
Source	R_T **[-]**	**Error [-]**	T_T **[-]**	**Error [-]**
Giovanelli [14]	0.2600	-	-	-
Prahl et al. [15]	0.2607	0.00170	-	-
Our model	0.2605	0.00038	-	-
Case 2				
van der Hulst [13]	0.09734	-	0.66096	-
Prahl et al. [15]	0.09711	0.00033	0.66159	0.00049
Our model	0.09682	0.00036	0.66163	0.00041

E. Experiments

Blood vessel positions were simulated to investigate their influence on the detected PPG signal (see Fig. 1). Regular and dilated blood vessel states were simulated for every vessel position. The source and detector edge-to-edge distance was 3.00 mm. The circular source had a diameter of 0.5 mm and the square detector had a surface area of 1x1 mm. The simulated wavelengths were 660 nm and 940 nm. Simulations were repeated five times with 10^8 photon packets each.

III. RESULTS

A. Validation

The developed MC simulation framework is in agreement with reference values taken from literature within limits of error. Details are show in Tab. II.

B. Variation of blood vessel position

Detected photon count decreased towards a centered arrangement of the PPG sensor above the blood vessel (see Fig. 2A). Vessel dilation and wavelength did not influence the photon count trend towards the centered arrangement. Median count of detected photon packets decreased with centered sensor positioning above the blood vessel (Vessel pos. C) for both wavelengths, independent of vessel dilation. Blood absorbed between 1.4% and 7.0% at 660 nm and 2.4% and 14.5% at 940 nm of the photon packet weight (see Fig. 2C). The more centered the sensor was positioned over the blood vessel, the more photon packet weight was absorbed by blood. A similar effect occurred in the tissue vessel wall. Skin layers *Epidermis*, *Upper blood net*, *Reticular dermis*, *Deep blood net dermis* and *Subcutaneous fat* showed an opposite effect compared to blood: Here, results were independent of the wavelength and vessel dilation. The relative signal difference (see Fig. 2D) showed that the centered sensor positioning above the blood vessel was most effective. Hence the relative signal difference pattern is in agreement with the absorption results for blood and vessel walls. Median maximum penetration depth per sensor position (see Fig. 2B) increased towards the centered arrangement (Vessel pos. C) for 660 nm and decreased for 940 nm, independent of vessel dilation.

IV. DISCUSSION

Detected photon packets pass through tissue in a banana curve depending on wavelength [16], as shown in Fig 3. For example, at 530 nm (green light) average penetration depth was only 0.3 mm [11] and therefore was not investigated in our present work. We observed lower penetration depth at 940 nm, which indicates a sub-optimal source-detector distance compared to 660 nm (see Fig. 3). The blood vessel absorbs photon packets and decreases their weight. The further a blood vessel reaches into the banana curve of photon packets, the more it influences the detected photon packets. Due to the high absorption and scattering of vessel wall and blood (see Fig. 2C), fewer photon packets with less photon weight hit the detector for 660 nm compared to 940 nm (see Fig. 2A). Due to a reduced average penetration, the banana curve at 660 nm did not extend as far into the blood vessel as for 940 nm. Consequently, the blood vessel influences detected photon packets depending on its depth and position. The effect's intensity is wavelength-dependent (due to penetration depth) as well as depending on scattering and absorption properties. Moreover, median maximum penetration depth across vessel positions showed an increase in penetration depth at 660 nm and a decrease at 940 nm towards the centered position (Pos. C). The result suggests that larger source-detector distances at 940 nm are needed. Blood perfusion in skin layers and varying vessel depth were not considered in our simulation, which however may influence penetration depth.

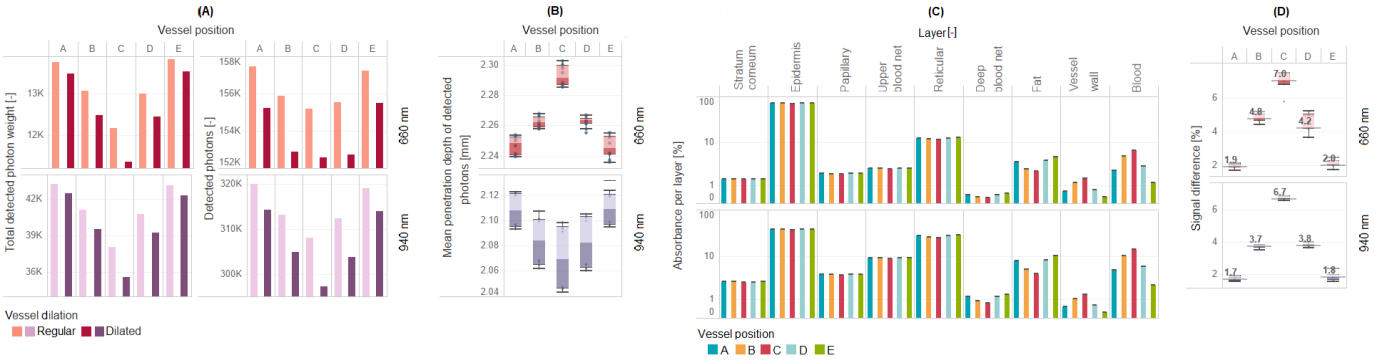

Fig. 2. Simulation results for wavelengths of 660 nm and 940 nm, including non-dilated and dilated blood vessels. (A) Left: Total detected photon packets. Right: Number of detected photon packets (B) Average maximum penetration depth. Dashed lines indicate median maximum penetration depth. (C) Percentage absorption of *Stratum corneum*, *Epidermis*, *Papillary dermis*, *Upper blood net dermis*, *Reticular dermis*, *Deep blood net dermis*, *Subcutaneous fat*, *Vessel wall* and *Blood*. (D) Signal difference between regular and dilated vessel.

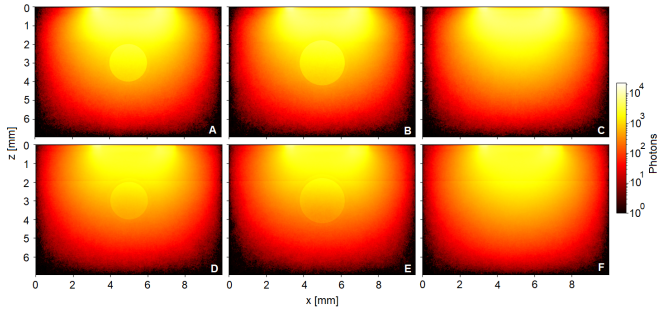

Fig. 3. Summed trajectories of detected photon packets at 660 nm (Plots A-C) and 940 nm (Plots D-F). (A,D): Regular blood vessel. (B, E): Dilated blood vessel. (C,F): Simulation without blood vessel.

PPG signal variations observed in static and alternating signals range from 0.01% to 10% [17]. Our results identify a substantial variation related to vessel positioning (see Fig. 2D). Moreover, dilation increases the photon packet count reaching a blood vessel. As more photon packets hit a blood vessel, signal difference between regular and dilated state increases.

V. Conclusion

The connection of signal quality and PPG sensor position around a blood vessel was analysed. To maximise the PPG signal, light source and detector should be symmetrically placed over a large blood vessel. Our simulation method can be used to optimise PPG sensor positioning.

References

[1] M. Ghamari, "A review on wearable photoplethysmography sensors and their potential future applications in health care," Int. J. Biosens. Bioelectron., vol. 4, no. 4, 2018, doi: 10.15406/ijbsbe.2018.04.00125.

[2] R. R. Anderson and J. A. Parrish, "The Optics of Human Skin," J. Invest. Dermatol., vol. 77, no. 1, pp. 13–19, Jul. 1981, doi: 10.1111/1523-1747.ep12479191.

[3] L. Wang, S. L. Jacques, and L. Zheng, "MCML—Monte Carlo modeling of light transport in multi-layered tissues," Comput. Methods Programs Biomed., vol. 47, no. 2, pp. 131–146, Jul. 1995, doi: 10.1016/0169-2607(95)01640-F.

[4] Q. Fang and D. A. Boas, "Monte Carlo simulation of photon migration in 3D turbid media accelerated by graphics processing units," Opt. Express 17, 20178-20190 (2009).

[5] I. V. Meglinski and S. J. Matcher, "Quantitative assessment of skin layers absorption and skin reflectance spectra simulation in the visible and near-infrared spectral regions," Physiol. Meas., vol. 23, no. 4, pp. 741–753, Nov. 2002, doi: 10.1088/0967-3334/23/4/312

[6] X.-B. D. Pham et al., "Racial and Gender Differences in Arterial Anatomy of the Arm," Am. Surg., vol. 82, no. 10, pp. 973–976, Oct. 2016.

[7] T. Boonya-ananta et al., "Synthetic photoplethysmography (PPG) of the radial artery through parallelized Monte Carlo and its correlation to body mass index (BMI)," Sci. Rep., vol. 11, no. 1, pp. 1–11, Jan. 2021, doi: 10.1038/s41598-021-82124-4.

[8] J. U. Kim, Y. J. Lee, J. Lee, and J. Y. Kim, "Differences in the Properties of the Radial Artery between Cun, Guan, Chi, and Nearby Segments Using Ultrasonographic Imaging: A Pilot Study on Arterial Depth, Diameter, and Blood Flow," Evid. Based Complement. Alternat. Med., vol. 2015, pp. 1–7, 2015, doi: 10.1155/2015/381634.

[9] L. C. Henyey and J. L. Greenstein, "Diffuse radiation in the galaxy," Astrophys. J., vol. 93, p. 70, Jan. 1941, doi: 10.1086/144246.

[10] V. V. Tuchin, Tissue Optics: Light scattering methods and instruments for medical diagnosis. Society of Photo-Optical Instrumentation Engineers (SPIE), 2015.

[11] S. Chatterjee, K. Budidha, and P. A. Kyriacou, "Investigating the origin of photoplethysmography using a multiwavelength Monte Carlo model," Physiol. Meas., vol. 41, no. 8, p. 084001, Sep. 2020, doi: 10.1088/1361-6579/aba008.

[12] N. Bosschaart, G. J. Edelman, M. C. G. Aalders, T. G. van Leeuwen, and D. J. Faber, "A literature review and novel theoretical approach on the optical properties of whole blood," Lasers Med. Sci., vol. 29, no. 2, pp. 453–479, Mar. 2014, doi: 10.1007/s10103-013-1446-7.

[13] H. Van de Hulst, Multiple light scattering. Elsevier, 1980. Accessed: May 27, 2022.

[14] R. G. Giovanelli, "Reflection by semi-infinite diffusers," Opt. Acta Int. J. Opt., vol. 2, no. 4, pp. 153–162, Dec. 1955, doi: 10.1080/713821040.

[15] S. A. Prahl, "A Monte Carlo model of light propagation in tissue," Jan. 1989, p. 1030509. doi: 10.1117/12.2283590.

[16] C. Mansouri and N. H., "New Window on Optical Brain Imaging; Medical Development, Simulations and Applications," in Selected Topics on Optical Fiber Technology, M. Yasin, Ed. InTech, 2012.

[17] T. Tamura, "Current progress of photoplethysmography and SPO2 for health monitoring," Biomed. Eng. Lett., vol. 9, no. 1, pp. 21–36, Feb. 2019, doi: 10.1007/s13534-019-00097-w.